BIOCHEMISTRY
including biophysical chemistry & molecular biology
Article

Biochemistry **2009,** *48,* 11699–11705 11699
DOI: 10.1021/bi901517n

Interaction between Na^+ Ion and Carboxylates of the PomA−PomB Stator Unit Studied by ATR-FTIR Spectroscopy†

Yuki Sudo,[‡,§,⊥] Yuya Kitade,[∥,⊥] Yuji Furutani,[∥] Masaru Kojima,[‡] Seiji Kojima,[‡] Michio Homma,*[,‡] and Hideki Kandori*[,∥]

[‡]*Division of Biological Science, Graduate School of Science, Nagoya University, Chikusa-ku, Nagoya 464-8602, Japan,* [§]*PRESTO, Japan Science and Technology Agency (JST), 4-1-8 Honcho Kawaguchi, Saitama 332-0012, Japan, and* [∥]*Department of Frontier Materials, Nagoya Institute of Technology, Showa-ku, Nagoya 466-8555, Japan*
[⊥]*These authors equally contributed to this work.*

Received August 29, 2009; Revised Manuscript Received November 5, 2009

ABSTRACT: Bacterial flagellar motors are molecular machines powered by the electrochemical potential gradient of specific ions across the membrane. The PomA−PomB stator complex of *Vibrio alginolyticus* couples Na^+ influx to torque generation in this supramolecular motor, but little is known about how Na^+ associates with the PomA−PomB complex in the energy conversion process. Here, by means of attenuated total reflection Fourier-transform infrared (ATR-FTIR) spectroscopy, we directly observed binding of Na^+ to carboxylates in the PomA−PomB complex, including the functionally essential residue Asp24. The Na^+ affinity of Asp24 is estimated to be ~85 mM, close to the apparent K_m value from the swimming motility of the cells (78 mM). At least two other carboxylates are shown to be capable of interacting with Na^+, but with somewhat lower affinities. We conclude that Asp24 and at least two other carboxylates constitute Na^+ interaction sites in the PomA−PomB complex. This work reveals features of the Na^+ pathway in the PomA−PomB Na^+ channel by using vibrational spectroscopy.

Bacterial flagellar motors are classified by the coupling ion, Na^+ or H^+. *Escherichia coli* has H^+-driven flagellar motors, whereas the polar flagella of marine *Vibrio* species have Na^+-driven motors (*1*−*3*). The transmembrane proteins PomA[1] and PomB of *Vibrio alginolyticus* form stator complexes essential for the motility of the bacterium (*1*, *4*). Purified PomA−PomB complexes reconstituted into proteoliposomes were shown to have sodium-conducting activity (*5*), implying that this complex is sufficient for conduction of Na^+. It is believed that ion flux drives the interactions and structural changes between the PomA−PomB complex and a rotor protein in the C-ring, FliG (Figure 1A) (*2*). Thus, the ion flux mechanism through the PomA−PomB stator unit has become a focus of great interest, in part because of its importance to the general understanding of ion flux in ion channels (*6*). However, the mechanism of ion flow is still unclear.

Stimulus-induced difference Fourier-transform infrared (FTIR) spectroscopy is a powerful tool for investigating protein structural changes accompanying biologically important functional processes. This method has been extensively applied to photoactive proteins (*7*−*10*) and has been shown to allow detailed structural analysis, including changes in hydrogen bonding of even a single water molecule (*11*). This technique has not been as easily applied for other stimuli such as ion binding. Attenuated total reflection (ATR) FTIR uses samples that are filled in aqueous solution, so that solution pH and ionic composition, and transmembrane voltage, can be preserved and accurately controlled (*12*, *13*). Here we apply ATR-FTIR spectroscopy in investigating Na^+ binding to the membrane-embedded PomA−PomB complex.

Only one conserved carboxylic acid residue, Asp24 of PomB, is located within the predicted transmembrane regions of PomA and PomB (Figure 1 of the Supporting Information). Because a D24N mutant (*14*) is unable to rotate its flagella, Asp24 has been proposed to form a functionally important Na^+ binding site in the motor. However, no direct evidence of this interaction has been obtained, and relatively little detailed structural information is available for either the PomA−PomB complex or its H^+ conducting counterpart MotA−MotB. Here we investigate binding of Na^+ to Asp24 by comparing the infrared absorbance spectra of wild-type and D24N PomA−PomB complexes, purified and reconstituted into liposomes.

MATERIALS AND METHODS

Bacterial Strains, Plasmids, Media, and Growth Conditions. *E. coli* strain DH5α was used for DNA manipulations. *V. alginolyticus* strain NMB191 (Δ*pomAB*) (*15*) was used in this study for the swimming assay and protein expression. Mutant genes were constructed by PCR using the QuikChange site-directed mutagenesis method. For the measurements of swimming speed, an overnight culture of *V. alginolyticus* in VC medium was incubated in VPG500 medium (1% polypeptone,

†This work was supported in part by grants from Japanese Ministry of Education, Culture, Sports, Science, and Technology to Y.S. (20050012), Y.F. (19042013 and 19045015), S.K. (18770129), M.H. (18207011), and H.K. (2050015 and 20108014).

*To whom correspondence should be addressed. M.H.: telephone, +81 (52) 789-2991; fax, +81 (52) 789-3001; e-mail, g44416a@cc.nagoya-u.ac.jp. H.K.: telephone and fax, +81-52-735-5207; e-mail, kandori@nitech.ac.jp.

[1]Abbreviations: PomA, polar flagellar motility protein A; PomB, polar flagellar motility protein B; FTIR, Fourier transform infrared; ATR, attenuated total reflection.

Published on Web 11/07/2009

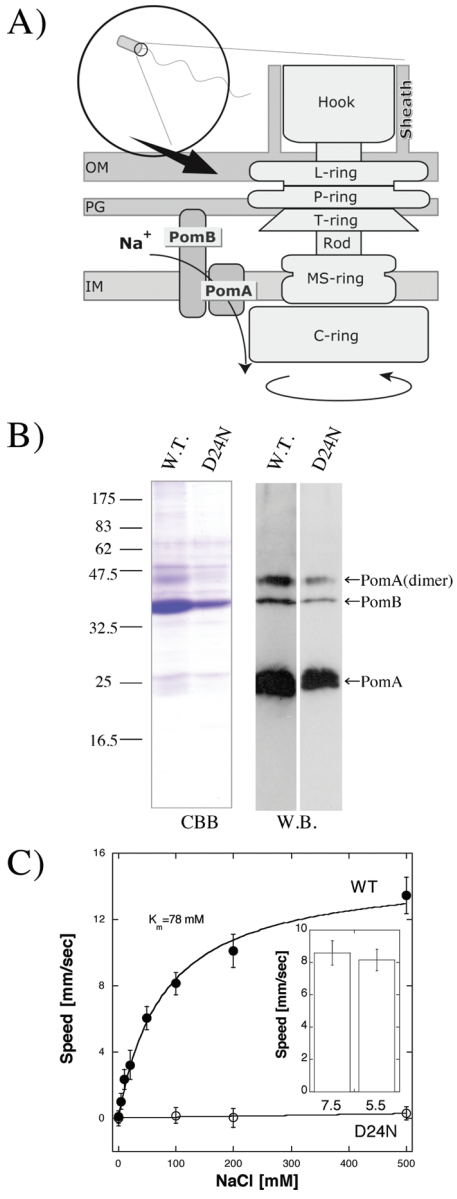

FIGURE 1: (A) Hypothetical model for the sodium-driven motor in *V. alginolyticus*. The flagellar motor was composed of L-ring, P-ring, T-ring, MS-ring, C-ring, hook, rod, and stator proteins, PomA and PomB. The energy source for the flagellar motor rotation is provided by an electrochemical potential gradient across the inner membrane. Here the PomA−PomB complex forms a Na^+ channel and plays an important role in torque generation. IM, PG, and OM denote the inner membrane, peptidoglycan, and outer membrane, respectively. (B) SDS−PAGE patterns of the purified Cys-less PomA−PomB (W.T.) and Cys-less PomA−PomB-D24N complex (D24N) by CBB staining (CBB), and immnoblotting analysis of PomA and PomB (WB). Proteins were detected with an anti-PomA1312 antibody and anti-PomB93 antibody. (C) Estimation of apparent Na^+ binding affinity with the Cys-less PomA−PomB (W.T.) and Cys-less PomA−PomB-D24N complex (D24N). *V. alginolyticus* strain NMB191 (△*pomAB*) (*15*) was used here for the swimming assay. The swimming speed of the cells was measured at pH 5.5 in the TMN medium containing various concentrations of NaCl (ionic strength kept constant at 500 mM with KCl), and it was plotted vs NaCl concentration. The data of the Cys-less PomA−PomB complex (W.T.) were fitted with a Michaelis−Menten equation with a K_m and a V_{max} of 78 ± 10 mM and 15 ± 1 μm/s, respectively. The D24N mutant shows no motile behavior as reported previously (*14*). The swimming speed of the cells was also measured at pH 7.5 in the buffer containing 50 mM Tris (pH 7.5), 5 mM $MgSO_4$, 5 mM glucose, 100 mM NaCl, and 400 mM KCl, and it was compared with the value estimated at pH 5.5 (inset).

0.4% K_2HPO_4, 500 mM NaCl, and 0.5% glycerol) at a 100-fold dilution, and cells were grown at 30 °C to exponential growth phase. Cells were centrifuged at 3500*g* for 3 min, and the sedimented cells were resuspended in TMN50 [50 mM BisTris (pH 5.5), 5 mM $MgSO_4$, 5 mM glucose, 50 mM NaCl, and 450 mM KCl]. Cell suspensions were diluted 50-fold into TMN medium containing various concentrations of NaCl (ionic strength kept constant at 500 mM with KCl), and the motilities of cells were observed immediately using a dark-field microscope. Swimming speeds were determined from at least 200 individual cells as described previously (*16*, *17*). Briefly, the speeds were calculated from individual cell tracks measured by a computer-assisted motion analysis program. The constructed plasmids were confirmed using an automated sequencer. For protein expression, *V. alginolyticus* cells were cultured at 30 °C in VC medium (0.5% polypeptone, 0.5% yeast extract, 0.4% K_2HPO_4, 3% NaCl, and 0.2% glucose). When necessary, kanamycin was added to a final concentration of 100 μg/mL.

Protein Expression, Purification, and Reconstitution into E. coli Polar Lipids. A plasmid that overproduces the PomA−PomB complex with six histidine residues at the C-terminus of PomB was used here. Cys-less PomA−PomB (C8A-PomB, C10A-PomB, and C31A-PomB) and Cys-less PomA−PomB-D24N were used in this study to avoid the unexpected formation of an oligomer (dimer, tetramer, etc.) during the purification in the detergent and reconstitution into liposomes. Purification of the PomA−PomB complex was conducted as described previously (*5*). Briefly, the membrane fraction was solubilized with 2.5% (w/v) CHAPS in a buffer containing 20 mM Tris-HCl (pH 8.0), 150 mM NaCl, 20 mM imidazole, 10% (w/v) glycerol, 5 mM $MgCl_2$, and 1 tablet of Complete EDTA-free protease inhibitor cocktail (Roche Applied Science, Indianapolis, IN). After ultracentrifugation, the supernatant was applied to a Ni-affinity column (HisTrap, GE) in a buffer containing 20 mM Tris-HCl (pH 8.0), 150 mM NaCl, 20 mM imidazole, 10% (w/v) glycerol, 5 mM $MgCl_2$, and 1 tablet of Complete EDTA-free protease inhibitor cocktail. The eluted sample was further purified with an ion-exchange column (HiTrapQ, GE) and a gel-filtration column, with Superdex 200HR (Amersham Biosciences, Pittsburgh, PA) in the same buffer described above. Finally, 2.8 mg of protein for Cys-less PomA−PomB and 1.8 mg of protein for Cys-less PomA−PomB-D24N were obtained from a 140 L culture. The purified sample was then mixed with *E. coli* polar lipids (Avanti Polar Lipids, Alabaster, AL), where the molar ratio of added lipids to PomA−PomB complex was 30, and it was incubated at room temperature for 1 h. Then, the detergent was removed by dialysis against 20 mM Tris-HCl (pH 6.8), 150 mM KCl, 10% (w/v) glycerol, and 5 mM $MgCl_2$ at room temperature overnight. Na^+ channel activity in the *E. coli* polar lipids was previously confirmed in ref *5*, and Yonekura et al. previously reported by using cryo-electron microscopy that the PomA forms a complex with PomB and that complex forms the structural unit in the proteoliposomes (*18*). The purified sample was dissolved in sodium dodecyl sulfate−polyacrylamide gel electrophoresis (SDS−PAGE) loading buffer containing 5% 2-mercaptoethanol and was subjected to SDS−PAGE. Immunoblotting was performed using an anti-PomA antibody (PomA1312) and an anti-PomB antibody (PomB93) as described previously (*15*).

Perfusion-Induced Attenuated Total Reflection (ATR) FTIR Spectroscopy. The PomA−PomB sample was placed on the surface of a diamond ATR crystal (SMITHS, nine effective

internal reflections). After drying in a gentle stream of N_2, the sample was rehydrated with perfusion buffer [50 mM BisTris (pH 5.5)]. Before Na^+-induced difference spectra were recorded, the film was perfused with the same buffer at a flow rate of 0.6 mL/min for 100 min. ATR-FTIR spectra of the PomA−PomB film were recorded at 293 K and 2 cm^{-1} resolution with a Bio-Rad FTS-6000 spectrometer, equipped with a liquid nitrogen-cooled MCT detector (*19*). A background spectrum of the film (an average of 512 interferograms) was first recorded during perfusion with buffer in the absence of NaCl. The buffer was then switched to that containing 100 mM NaCl, and after a 2 min delay for equilibration, a Na^+-binding minus Na^+-free difference spectrum was recorded (an average of 512 interferograms). Then, after a new background was taken, the buffer was switched back to that without NaCl, and after a 3 min delay, an equivalent Na^+-free minus Na^+-binding difference spectrum was recorded. The cycling procedure was repeated 8−16 times, and the difference spectra were calculated as averages of PomA−PomB(Na^+) minus PomA−PomB(free), and PomA−PomB(free) minus PomA−PomB(Na^+) spectra. The flow rate was maintained at 0.6 mL/min. PomA−PomB(Li^+, K^+, or Cs^+) minus PomA−PomB(free) spectra were measured with the same method (Figure 2 of the Supporting Information). It should be noted that the spectral changes thus obtained contain those of water molecules and buffer components in addition to the spectral changes of the PomA−PomB complex itself. Thus, we adopted the correction procedure to remove such spectral changes as described in the legend of Figure 2.

RESULTS

Protein Expression and Purification of the PomA−PomB Complex. Both PomA and PomB were unstable when expressed alone in *E. coli* and *V. alginolyticus*, mainly because of protein degradation. Therefore, we used here a plasmid encoding PomA with PomB, by which the functional protein complex was purified from native *V. alginolyticus* cells. In addition, Cys-less PomA−PomB complexes were used to prevent formation of cross-linked oligomers during purification and reconstitution into liposomes. WT and D24N contain 83 and 85% PomA−PomB proteins, respectively, estimated from the intensity of the bands of 14% acrylamide SDS−PAGE (Figure 1B, CBB). The protein expression is also confirmed by immunoblotting with anti-PomA and anti-PomB (Figure 1B, WB) (*15*). Figure 1C shows the swimming speeds of cells containing the WT or D24N PomA−PomB complex at varying NaCl concentrations. The data for WT fit well to the Michaelis−Menten equation, and the kinetic parameters, K_m and V_{max}, were determined to be 78 ± 10 mM and 15 ± 1 μm/s, respectively (Figure 1C). The D to N mutation of Asp24 destroyed the motility of the cells as reported previously (*14*).

Perfusion-Induced ATR-FTIR Spectroscopy with and without NaCl. In the ATR-FTIR measurements, purified proteins were reconstituted into proteoliposomes and dried on an ATR diamond cell. Then, Na^+-free and Na^+-containing (100 mM) buffers at pH 5.5 were alternatively perfused, as IR absorptions were monitored under each buffer condition. We confirmed that the PomA−PomB(Na^+) minus PomA−PomB(free) and PomA−PomB(free) minus PomA−PomB(Na^+) spectra represent mirror images of each other, so that the measurements could be replicated by changing buffers repeatedly. The obtained difference spectra contain features due to water molecules and buffer components in addition to those of the PomA−PomB complex itself (see Materials and Methods). These were removed using a correction procedure described in the legend of Figure 2. The corrected PomA−PomB(Na^+) minus PomA−PomB(free) difference spectrum exhibits peaks at 1720 (−), 1651 (−), 1576 (+), and 1401 (+) cm^{-1}, presumably originating from the binding of Na^+ to the PomA−PomB complex (Figure 2C).

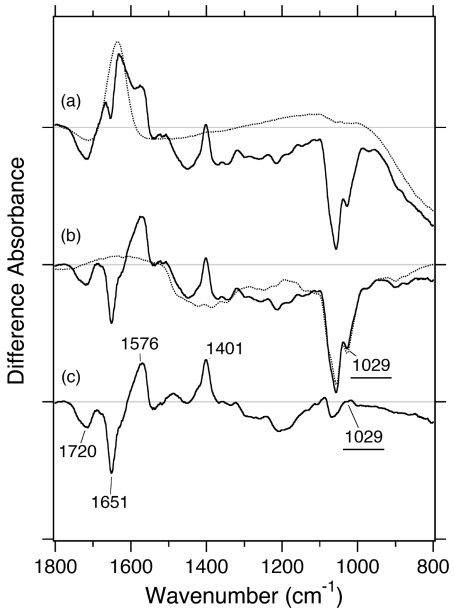

FIGURE 2: Difference ATR-FTIR spectra for the binding of Na^+ to the PomA−PomB complex at pH 5.5 and 293 K. One division of the *y*-axis corresponds to 0.005 absorbance unit. (A) The solid line represents the difference spectrum for the PomA−PomB complex between the presence and absence of Na^+ in the buffer (100 mM NaCl), where positive and negative signals correspond to Na^+-bound and Na^+-free forms, respectively. Note that the spectral changes contain those of water molecules and buffer components in addition to the spectral changes of the PomA−PomB complex itself, which is removed as follows. First, we attempted to remove the contribution of water molecules. The dotted lines show the difference spectra measured under the identical conditions without the PomA−PomB sample, where positive and negative signals correspond to 100 and 0 mM NaCl, respectively. These difference spectra originate from spectral changes of water molecules induced by binding of NaCl, as evidenced by a positive O−H bending vibration at ~1630 cm^{-1} and negative vibrations at 1000−800 cm^{-1}. By subtracting the contribution of water molecules, we obtained the difference spectrum (solid line in panel B). (B) The solid line is the difference ATR-FTIR spectrum after subtraction of the water contribution. Note that the spectrum contains the signals of the buffer, as the different salt conditions (0 and 100 mM NaCl) appear to change the sample conditions, such as the thickness or density of the liposome layer adsorbed on the ATR crystal, so that less buffer is observed in the presence of Na^+. The dotted line in panel B represents the difference spectrum between 0 and 2 mM BisTris at pH 5.5 after subtraction of the water contribution, where sharp peaks at 1100−1000 cm^{-1} originate from the infrared absorption of BisTris. (C) Difference ATR-FTIR spectrum for binding of Na^+ to the PomA−PomB complex obtained by subtracting the dotted line from the solid line in panel B. The positive and negative signals correspond to Na^+-bound and Na^+-free forms, respectively. The present correction of the buffer contribution may not be quantitative, but peaks due to water molecules (dotted line in panel A) and the buffer (dotted line in panel B) are broader than those originating from the PomA−PomB complex (panel C). In addition, important bands, such as a negative band at 1720 cm^{-1} and a positive band at 1401 cm^{-1}, are detectable even in the raw data (solid line in panel A). Thus, it is safe to assume that the spectrum in panel C represents the PomA−PomB(Na^+) minus PomA−PomB(free) difference ATR-FTIR spectrum.

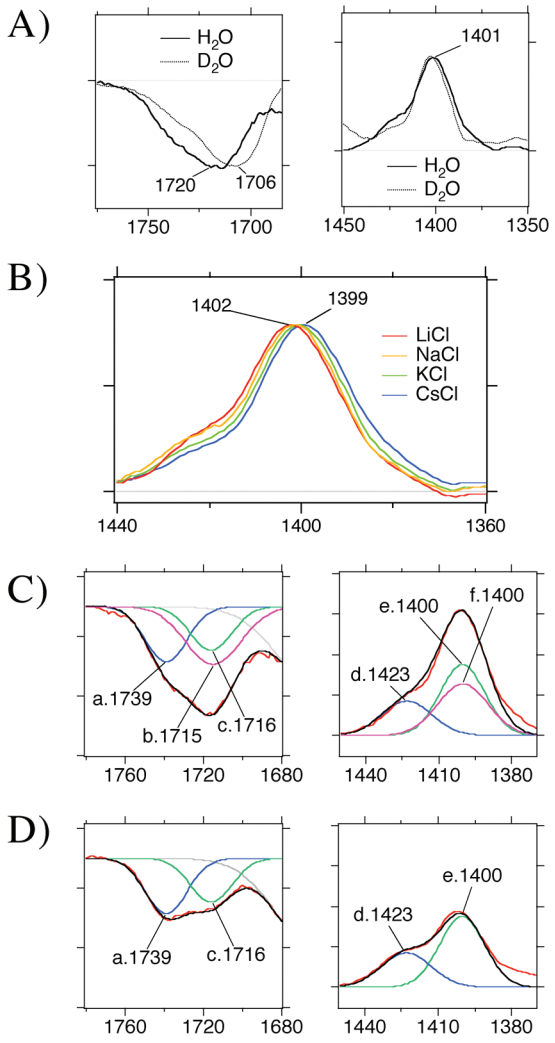

FIGURE 3: PomA−PomB(Na^+) minus PomA−PomB(free) difference ATR-FTIR spectra for Cys-less PomA−PomB from *V. alginolyticus* measured at 293 K. The buffer contains 0 or 100 mM NaCl at pH 5.5. (A) PomA−PomB(Na^+) minus PomA−PomB(free) spectra in the COOH (left) and symmetric COO^- (right) stretching vibrational regions. The H_2O (—) or D_2O (···) buffers are used. (B) ATR-FTIR difference spectra of the PomA−PomB complex in the symmetric COO^- stretching region measured in the presence of 100 mM LiCl (red), NaCl (orange), KCl (green), or CsCl (blue). (C) Deconvolution of the COOH (left) and symmetric COO^- (right) stretching bands in the PomA−PomB(Na^+) minus PomA−PomB(free) spectra of WT. The data (red curves) were fitted by the sum (black curves) of three components of Gaussian distributions (blue, green, and pink curves). Numbers in the figure represent peak frequencies of each Gaussian function. One division of the *y*-axis corresponds to 0.0005 absorbance unit. (D) Deconvolution of the COOH (left) and symmetric COO^- (right) stretching bands in the PomA−PomB(Na^+) minus PomA−PomB(free) spectra of D24N. The data (red curves) were fitted by the sum (black curves) of two components of Gaussian distributions (blue and green curves), which are reproduced from Figure 3C (blue and green curves) with the same relative intensities. One division of the *y*-axis corresponds to 0.0005 absorbance unit.

COOH and COO^- Vibrations of Carboxylic Acid Residues. The frequencies at 1720 (−), 1576 (+), and 1401 (+) cm^{-1} in Figure 2C are characteristic of protonated carboxylic C=O stretching and carboxylate asymmetric and symmetric stretching vibrations, respectively. This suggests that binding of Na^+ to the PomA−PomB complex is accompanied by deprotonation of carboxylate(s). In fact, the frequency at 1720 (−) cm^{-1} is downshifted to 1706 (−) cm^{-1} in D_2O (Figure 3A, left), but that at 1401 (+) cm^{-1} is little influenced in D_2O (Figure 3A, right). The D_2O sensitivities of the bands at 1720 (−) and 1401 (+) cm^{-1} are typical for a protonated and unprotonated carboxylate, respectively. Since the band at 1576 cm^{-1}, carboxylate asymmetric stretching vibration, appears in the frequency region of amide II and side chain vibrations, spectral features were complex for the detailed analysis. We thus applied the analysis in Figures 3 and 4 to the bands at 1720 and 1401 cm^{-1} in this study. Carboxylic acid deprotonation upon Na^+ binding is further supported by the fact that the frequency of the 1401 cm^{-1} (+) band shifts systematically to a lower energy as the cation mass is increased (Figure 3B), where the difference spectra for LiCl, KCl, and CsCl were similarly obtained as shown in Figure 2 of the Supporting Information. The cation dependence was not observed for the negative band at 1720 cm^{-1} (Figure 3 of the Supporting Information), consistent with its assignment to the protonated rather than cation-bound form. Thus, it is evident that some carboxylates in the PomA−PomB complex are protonated in the absence of Na^+ but form ion pairs with Na^+ in buffer containing 100 mM NaCl (pH 5.5). The frequency difference (175 cm^{-1}) between asymmetric (1576 cm^{-1}) and symmetric (1401 cm^{-1}) stretching vibrations is in line with the carboxylate(s) coordinating to Na^+ as a bidentate ligand, in which the two oxygen atoms are similar distances from Na^+ (*20*).

The negative band at 1720 cm^{-1} (Figure 3A, left) is relatively broad, and the positive band at 1401 cm^{-1} (Figure 3A, right) has a shoulder on the higher-frequency side, suggesting the contribution of multiple carboxylates. The negative and positive bands in Figure 3A were fitted well by the sum of three Gaussian components (Figure 3C, left and right, respectively). Two components may be satisfactory in describing the spectral shapes at high Na^+ concentrations but did not adequately account for Na^+ concentration dependencies, as detailed below. This indicates that three carboxylates participate in Na^+ binding in the PomA−PomB complex. In the D24N mutant (see Figure 4 of the Supporting Information for the full spectra), the bands showed changes consistent with the loss of the component absorbing at 1715 and 1400 cm^{-1} (Figure 3D). This result provides the first evidence that Asp24 becomes deprotonated in the presence of Na^+, presumably being displaced by Na^+. Figure 3D also shows that the two remaining carboxylates possess protonated carboxylic vibrations at 1739 (curve a) and 1716 cm^{-1} (curve c) and symmetric COO^- stretching vibrations at 1423 (curve d) and 1400 cm^{-1} (curve e).

Estimation of Dissociation Constants for Na^+. To estimate the dissociation constants for Na^+, we next measured ATR-FTIR spectra at various NaCl concentrations (5, 10, 20, 50, 100, and 200 mM), at pH 5.5 and a temperature of 293 K (Figure 4A). The WT minus D24N difference spectra are shown in the right panel. The WT, D24N mutant, and WT minus D24N difference spectra were fitted well by three-, two-, and one-component Gaussian distributions, respectively, with the same maximum (i.e., at saturating Na^+) intensities. The magnitude of each component was plotted versus the NaCl concentration to produce estimates of the dissociation constant K_d for each site (Figure 4B). The K_d values for binding of Na^+ to Asp24 were estimated to be 98 mM (1715 cm^{-1} band, curve b in Figure 3C) and 85 mM (1400 cm^{-1} band, curve f in Figure 3C). Dissociation constants for the other carboxylates were estimated to be 121 and 120 mM using the 1739 and 1716 cm^{-1} features, respectively (curves a and c in Figure 3C,D) and at 142 and 117 mM using the 1423 and 1400 cm^{-1} features, respectively (curves d and e in Figure 3C,D).

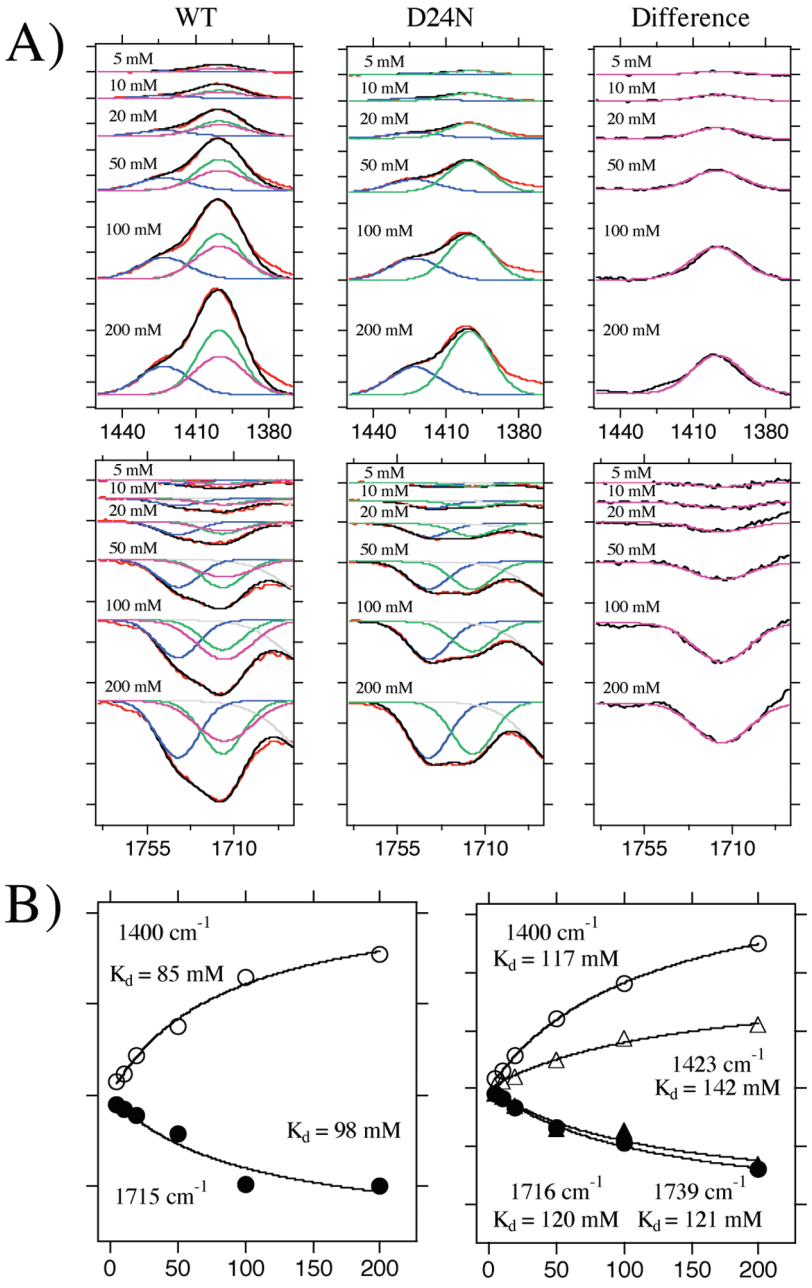

FIGURE 4: (A) PomA−PomB(Na^+) minus PomA−PomB(free) difference ATR-FTIR spectra for the Cys-less PomA−PomB complex from *V. alginolyticus* at the varying NaCl concentrations (5, 10, 20, 50, 100, and 200 mM). WT minus D24N difference spectra are shown in the right panel. Top and bottom panels represent the analysis of the symmetric COO^- and COOH stretching vibrational regions, respectively. The curve fitting procedure is the same as that described in the legend of Figure 3C,D. One division of the *y*-axis corresponds to 0.0005 absorbance unit. (B) Estimation of the binding affinity of Na^+ for Asp24 (left) and the other two carboxylates (right). The data of Asp24 bands at 1400 cm^{-1} (Figure 4A, top, right) and 1715 cm^{-1} (Figure 4A, bottom, right) were fitted to a one-binding site model with a K_d of 85 mM for a 1400 cm^{-1} band and a K_d of 98 mM for a 1715 cm^{-1} band. The data of the other two carboxylate bands were also fitted to a one-binding site model. One division of the *y*-axis corresponds to 0.0005 absorbance unit.

The affinity of Na^+ for Asp24 is slightly higher than for the other carboxylates and is close to the apparent K_m estimated from swimming speed measurements [78 mM (Figure 1C)]. The results further indicate that mutation of Asp24 does not markedly affect the Na^+ affinity of the other two sites.

DISCUSSION

In analogy to the proposed model for the MotA−MotB complex (*21*), the single TM of PomB and TM3 and TM4 of PomA are suggested to constitute most of the Na^+ channel in the $PomA_4PomB_2$ complex (Figure 1 of the Supporting Information). This study suggests that transported Na^+ ions are bound to Asp24 during its conduction process. Then, the mechanism for the interaction between Na^+ and Asp24 is intriguing. The observed frequency difference between asymmetric (1576 cm^{-1}) and symmetric (1401 cm^{-1}) stretching vibrations (Figure 2C of the Supporting Information) is most consistent with a bidentate ligation of Na^+ to Asp24 (*20*), thus probably excluding other hydrogen bonds to the Asp side chain in the Na^+-bound state.

Besides Asp24, there are two other Na^+ sites in the PomA−PomB complex, hereafter termed sites A and B. Since the bands for sites A and B are not influenced by the D24N mutation (Figure 3D), there appears to be no conformational coupling

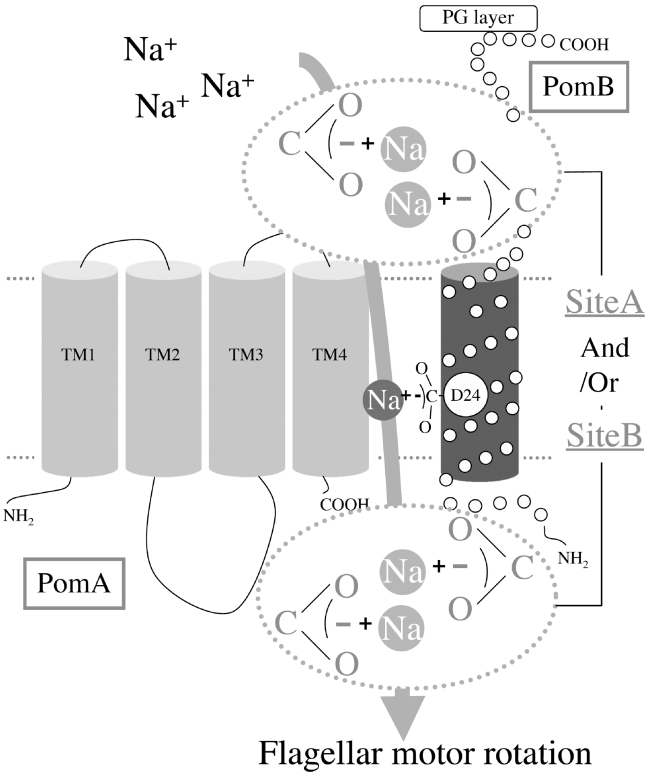

FIGURE 5: Model of the ion flux pathway in the PomA−PomB complex. Asp24 of PomB forms a Na^+ binding site in a chelating ligand manner. Two additional Na^+ binding sites are located at the surface of the PomA−PomB complex. The ion flux leads to interaction changes and structural change(s) of a rotator C-ring component protein FliG, and they mediate the flagellar motor rotation.

between these carboxylates. Ion flux probably changes the structure of the PomA−PomB complex, applying force to the C-ring component protein FliG (*3*). In this regard, a negative band at 1651 cm^{-1} in the PomA−PomB(Na^+) minus PomA−PomB(free) difference spectrum is particularly noted. The frequency is characteristic of an amide I vibration of an α-helix. Thus, the difference spectrum for binding of Na^+ to the PomA−PomB complex contains secondary structural information in addition to carboxylate vibrations, which will be analyzed in the future.

Sites A and B remain unidentified. Among the 81 carboxylates present in PomA and PomB (see Figure 1 of the Supporting Information), possible candidates include Asp31, Asp170, and Asp171, where mutations have been shown to affect swimming speed and/or Na^+ concentration dependencies. Then, where are site A and site B located? In this study, the ATR-FTIR spectra were recorded in a buffer at pH 5.5. Namely, it was predicted that the pK_a value of site A and site B is higher than 5.5, indicating the residues are in a hydrophobic environment. Kojima et al. reported that the motility of the D31C mutant of PomA exhibited a sharp dependence on NaCl concentration, with a threshold at 38 mM (*22*). D170C and D171C mutants of PomA show inhibition of the swimming motility, suggesting importance for the Na^+ flux (*1*). These three aspartates are predicted to lie on the periplasmic surface of the PomA−PomB complex where they might participate in the capture and delivery of Na to the channel, thus functioning as a Na^+ "antenna". If the carboxylates exist on the cytoplasmic side of the PomA−PomB complex, the residues should become the Na^+-unbound form because the concentration of Na^+ inside the cells is much lower than the K_d values estimated here (117−141 mM). Thus, we assume that a Na^+ antenna functionally exists at the periplasmic surface of the PomA−PomB complex. In fact, it was assumed that a segment of the MotB protein acts as a plug to prevent premature proton flow. The plug is in the periplasm just C-terminal to the MotB TM (*23*). On the basis of these results, we propose a Na^+ influx model in Figure 5. The Na^+−Asp24 interaction and Na^+ flow induce structural changes in the PomA−PomB complex to act on FliG and drive rotation, while sites A and B act as Na^+ antennae. To confirm the possibility, we constructed PomA-D31N−PomB, PomA-D170N−PomB, and PomA-D171N−PomB mutants. However, these mutant proteins exhibited dissociation between PomA and PomB during the purification; therefore, it was impossible to assign sites A and B. Technical advances should be required for the future experiments.

ACKNOWLEDGMENT

We thank Prof. David Blair for critical reading of the manuscript.

SUPPORTING INFORMATION AVAILABLE

Topology of PomA and PomB (Figure 1), ATR-FTIR spectra of the PomA−PomB complex in the presence of LiCl, KCl, and CsCl (Figure 2), ATR-FTIR spectra in the COOH stretching vibrational region (Figure 3), and ATR-FTIR spectra of the PomA−PomB-D24N complex (Figure 4). This material is available free of charge via the Internet at http://pubs.acs.org.

REFERENCES

1. Yorimitsu, T., and Homma, M. (2001) Na^+-driven flagellar motor of *Vibrio*. *Biochim. Biophys. Acta 1505*, 82–93.
2. Berg, H. C. (2003) The rotary motor of bacterial flagella. *Annu. Rev. Biochem. 72*, 19–54.
3. Blair, D. F. (2003) Flagellar movement driven by proton translocation. *FEBS Lett. 545*, 86–95.
4. McCarter, L. L. (2001) Polar flagellar motility of the Vibrionaceae. *Microbiol. Mol. Biol. Rev. 65*, 445–462.
5. Sato, K., and Homma, M. (2000) Functional reconstitution of the Na^+-driven polar flagellar motor component of *Vibrio alginolyticus*. *J. Biol. Chem. 275*, 5718–5722.
6. Fraser, S. P., and Pardo, L. A. (2008) Ion channels: Functional expression and therapeutic potential in cancer. Colloquium on Ion Channels and Cancer. *EMBO Rep. 9*, 512–515.
7. Kandori, H. (2004) Hydration switch model for the proton transfer in the Schiff base region of bacteriorhodopsin. *Biochim. Biophys. Acta 1658*, 72–79.
8. Sudo, Y., Furutani, Y., Spudich, J. L., and Kandori, H. (2007) Early photocycle structural changes in a bacteriorhodopsin mutant engineered to transmit photosensory signals. *J. Biol. Chem. 282*, 15550–15558.
9. Vogel, R., Sakmar, T. P., Sheves, M., and Siebert, F. (2007) Coupling of protonation switches during rhodopsin activation. *Photochem. Photobiol. 83*, 286–292.
10. Nabedryk, E., and Breton, J. (2008) Coupling of electron transfer to proton uptake at the Q(B) site of the bacterial reaction center: A perspective from FTIR difference spectroscopy. *Biochim. Biophys. Acta 1777*, 1229–1248.
11. Kandori, H. (2000) Role of internal water molecules in bacteriorhodopsin. *Biochim. Biophys. Acta 1460*, 177–191.
12. Vigano, C., Manciu, L., Buyse, F., Goormaghtigh, E., and Ruysschaert, J. M. (2008) Attenuated total reflection IR spectroscopy as a tool to investigate the structure, orientation and tertiary structure changes in peptides and membrane proteins. *Biopolymers 55*, 373–380.
13. Jiang, X., Zaitseva, E., Schmidt, M., Siebert, F., Engelhard, M., Schlesinger, R., Ataka, K., Vogel, R., and Heberle, J. (2008) Resolving voltage-dependent structural changes of a membrane photoreceptor by surface-enhanced IR difference spectroscopy. *Proc. Natl. Acad. Sci. U.S.A. 105*, 12113–12117.
14. Fukuoka, H., Wada, T., Kojima, S., Ishijima, A., and Homma, M. (2009) Sodium-dependent dynamic assembly of membrane

complexes in sodium-driven flagellar motors. *Mol. Microbiol. 71*, 825–835.
15. Yorimitsu, T., Sato, K., Asai, Y., Kawagishi, I., and Homma, M. (1999) Functional interaction between PomA and PomB, the Na^+-driven flagellar motor components of *Vibrio alginolyticus*. *J. Bacteriol. 181*, 5103–5106.
16. Sudo, Y., Furutani, Y., Kandori, H., and Spudich, J. L. (2006) Functional importance of the interhelical hydrogen bond between Thr204 and Tyr174 of sensory rhodopsin II and its alteration during the signaling process. *J. Biol. Chem. 281*, 34239–34245.
17. Sudo, Y., and Spudich, J. L. (2006) Three strategically placed hydrogen-bonding residues convert a proton pump into a sensory receptor. *Proc. Natl. Acad. Sci. U.S.A. 103*, 16129–16134.
18. Yonekura, K., Yakushi, T., Atsumi, T., Maki-Yonekura, S., Homma, M., and Namba, K. (2006) Electron cryomicroscopic visualization of PomA/B stator units of the sodium-driven flagellar motor in liposomes. *J. Mol. Biol. 357*, 73–81.
19. Kitade, Y., Furutani, Y., Kamo, N., and Kandori, H. (2009) Proton release group of *pharaonis* phoborhodopsin revealed by ATR-FTIR spectroscopy. *Biochemistry 48*, 1595–1603.
20. Deacon, G. B., and Phillips, R. J. (1980) Relationships between the carbon-oxygen stretching frequencies of carboxylato complexes and the type of carboxylate coordination. *Coord. Chem. Rev. 33*, 227–250.
21. Braun, T. F., Al-Mawsawi, L. Q., Kojima, S., and Blair, D. F. (2004) Arrangement of core membrane segments in the MotA/MotB proton-channel complex of *Escherichia coli*. *Biochemistry 43*, 35–45.
22. Kojima, S., Shoji, T., Asai, Y., Kawagishi, I., and Homma, M. (2000) A slow-motility phenotype caused by substitutions at residue Asp31 in the PomA channel component of a sodium-driven flagellar motor. *J. Bacteriol. 182*, 3314–3318.
23. Hosking, E. R., Vogt, C., Bakker, E. P., and Manson, M. D. (2006) The *Escherichia coli* MotAB proton channel unplugged. *J. Mol. Biol. 364*, 921–937.